Are We There Yet? A Critical Experimental Assessment of the Application of Induced Polarization for Monitoring Geochemical Processes

Strobel, C.; Störiko, A.; Cirpka, O. A.; Mellage, A.

DOI
10.1029/2024WR038567

Publication date
2025

Document Version
Final published version

Published in
Water Resources Research

Citation (APA)
Strobel, C., Störiko, A., Cirpka, O. A., & Mellage, A. (2025). Are We There Yet? A Critical Experimental Assessment of the Application of Induced Polarization for Monitoring Geochemical Processes. *Water Resources Research*, *61*(2), Article e2024WR038567. https://doi.org/10.1029/2024WR038567

Water Resources Research

RESEARCH ARTICLE
10.1029/2024WR038567

Are We There Yet? A Critical Experimental Assessment of the Application of Induced Polarization for Monitoring Geochemical Processes

C. Strobel[1,2], A. Störiko[3], O. A. Cirpka[1], and A. Mellage[2]

[1]Department of Geosciences, University of Tübingen, Tübingen, Germany, [2]Civil and Environmental Engineering, University of Kassel, Kassel, Germany, [3]Department of Water Management, Delft University of Technology, Delft, The Netherlands

Key Points:

- The (ad)sorption strength of the exchanging cation determines its effect on imaginary conductivity during cation exchange
- We propose separating the effect of ion exchange and salinity changes on the imaginary conductivity using a transport model
- The imaginary conductivity as a proxy for sorbed concentrations cannot replace geochemical samples

Supporting Information:

Supporting Information may be found in the online version of this article.

Correspondence to:

C. Strobel and A. Mellage,
cora.strobel@uni-tuebingen.de;
adrian.mellage@uni-kassel.de

Citation:

Strobel, C., Störiko, A., Cirpka, O. A., & Mellage, A. (2025). Are we there yet? A critical experimental assessment of the application of induced polarization for monitoring geochemical processes. *Water Resources Research*, *61*, e2024WR038567. https://doi.org/10.1029/2024WR038567

Received 2 AUG 2024
Accepted 10 DEC 2024

Author Contributions:

Conceptualization: C. Strobel, O. A. Cirpka, A. Mellage
Formal analysis: C. Strobel, A. Störiko
Funding acquisition: A. Mellage
Investigation: C. Strobel
Methodology: C. Strobel
Project administration: C. Strobel
Resources: O. A. Cirpka, A. Mellage
Software: C. Strobel, A. Störiko
Supervision: O. A. Cirpka, A. Mellage
Validation: C. Strobel
Visualization: C. Strobel
Writing – original draft: C. Strobel
Writing – review & editing: A. Störiko, O. A. Cirpka, A. Mellage

Abstract Spectral induced polarization (SIP) can provide valuable information about (bio)geochemical processes taking place in the poorly accessible subsurface. The method is sensitive to reactions that alter the solid-water interface. Here, we critically evaluate the effectiveness of SIP to monitor geochemical processes by focusing on a model-supported analysis of cation exchange dynamics in sediments containing organic matter. Organic matter is a crucial substrate for contaminant immobilization that exhibits a strong SIP response. We compare the SIP response of columns during the injection of cations (Na^+, Ca^{2+} and Zn^{2+}) with different sorption strengths. We assess whether a change in surface ion mobility due to cation exchange is reflected by an increasing (Na^+, high surface mobility) or decreasing (Zn^{2+}, low surface mobility) imaginary conductivity. Our work demonstrates how we can qualitatively monitor reactive solute fronts using (S)IP, thus, helping to target sampling events. Furthermore, we explore the quantitative value of SIP data sets in constraining reactive transport models. We use the imaginary conductivity as a proxy for sorbed concentrations by separating the contributions of ion exchange and bulk electrical conductivity to changes in imaginary conductivity. By integrating a Bayesian parameter-estimation scheme, we test whether the use of SIP can replace geochemical sampling and improve reaction-parameter estimates. While inverting SIP-data alone does not yield better results than breakthrough samples, their integration reduces the uncertainty of some parameters, highlighting their potential value. Finally, we discuss opportunities and limitations for reaction monitoring using SIP and provide an outlook for its successful application by non-geophysicists.

Plain Language Summary Understanding and monitoring geochemical processes in the subsurface is crucial for managing environmental challenges. However, the subsurface is difficult to access, and traditional sampling methods can be time-consuming and invasive. Spectral induced polarization (SIP) offers a promising alternative by providing indirect but detailed insights into these processes. It can detect changes in the electrical properties of sediment particles on which many critical reactions occur. This study investigates the potential of SIP to monitor the adsorption dynamics of cations as they flow through sediments containing organic matter (OM). OM is key for the immobilization of contaminants. By exploring how different cations (sodium, calcium and zinc) interact with OM and alter SIP signals, this research aims to assess SIP's ability to track reactive zones and enhance our understanding of geochemical reactions. We also explore whether SIP could replace traditional sampling methods and improve the accuracy of models used to predict contaminant transport in groundwater. Combining SIP data with traditional sampling helps to improve the accuracy of parameter predictions, showing SIP's potential as a complementary tool for environmental monitoring. Finally, we discuss how SIP could be more widely applied, even by non-specialists, while acknowledging its current limitations and areas for further development.

1. Introduction

Reactive processes in the subsurface are difficult to locate, identify and are very resource-intensive to monitor over time. Yet, they are key to understanding the fate of contaminants in the environment. Sorption on organic matter (OM) is of particular importance for contaminant transport in soils and sediments (Albers et al., 2009; Huang et al., 2003; Lair et al., 2007). The complexity of the OM composition and the lack of information on the concentrations in the sorbing phase (unless the solid phase is sacrificially sampled) often hamper the interpretation of column and field data. Reactive-transport models (RTMs) provide an approach to interpret experiments

despite the lack of data as they add theoretical knowledge of the reactive processes to the scarce data sets. They are thus a versatile tool to quantitatively bridge the gap between point measurements, validate the process comprehension, and predict the future behavior of the system under changing conditions (Li et al., 2021). Nevertheless, the lack of information on the solid-phase concentrations can impede the accurate determination of sorption parameters that are required to reliably upscale or extrapolate the findings of small-scale experiments.

The research fields of hydro- and bio-geophysics are evolving to complement traditional monitoring and modeling approaches with higher spatiotemporal resolution, potentially yielding deeper understanding of reactive processes in the hydrosphere (Atekwana & Slater, 2009; Kessouri et al., 2019). Especially the method of (spectral) induced polarization (SIP) has been applied to monitor various reactions at different scales. Examples include organic-contaminant sorption (Ben Moshe & Furman, 2022; Mellage, Zakai, et al., 2022), heavy-metal remediation (Bate et al., 2023; Flores Orozco et al., 2013), microbially mediated reactions (Mellage et al., 2018; Saneiyan, 2019; Strobel, Abramov, et al., 2023; Zhang et al., 2014), and plant root growth (Tsukanov & Schwartz, 2020; Weigand & Kemna, 2019). The advantage of SIP lies in its sensitivity to surface-related reactions, the non-invasiveness of the measurements, and the high temporal resolution combined with fast data acquisition. The potential of SIP lies therefore not only in complementing geochemical sampling of the pore water with information on the solid phase, but also in serving as a non-invasive, in-line monitoring tool. However, the latter requires that the processing and interpretation of the acquired SIP data is fast, straightforward, and independent of the geochemical sampling that often takes longer to be processed.

SIP is an active geoelectrical method in which an alternating current with defined frequency in the mHz to kHz range is injected into the sample through two current electrodes and the resulting impedance magnitude and phase shift are recorded between a second pair of potential electrodes (Binley & Slater, 2020). Within a single data-acquisition cycle, the frequency is tuned to achieve the response over an entire frequency range. The material property that is obtained from the raw measurements is typically expressed as a complex-valued electrical conductivity σ^* (S m^{-1}), in which the real part, σ', mainly depends on the electrical conduction through the pore fluid and along the grain-fluid interface (Slater & Glaser, 2003). The imaginary conductivity, σ'', is much smaller in magnitude than σ' and reflects electrical charge storage or surface polarization of the solid matrix. It also shows a stronger frequency dependence than σ', that can provide additional information on the length scale (distribution) of polarization (Schwarz, 1962). In the absence of metallic particles and within the low-frequency range (mHz to kHz), charge storage is controlled by electrochemical polarization of the electrical double layer (EDL). The EDL surrounds charged particles and essentially depends on the surface charge, the bulk fluid composition as well as the salinity and the chemical and electrostatic attraction between dissolved ions and the solid's surface. Under an applied electrical field, ions in the EDL and the corresponding counter ions in the bulk fluid migrate in response to the external field, causing the polarization around the particles, which alternates if an alternating current is injected. A key parameter that determines the magnitude of electrochemical polarization is the mobility of the counter ions in the EDL during the application of the electric field (Bücker et al., 2019; Leroy et al., 2008; Schwarz, 1962). The mobility of the ions in the EDL depends on their binding strength (both electrostatic and complexation) to the surface. Thus, σ'' is sensitive to reactions that alter the surface properties or the composition of the EDL, such as cation exchange and other sorption and sorption-like processes (e.g., precipitation and dissolution). Several studies have investigated the effect of different cations on the σ'' signal of mineral sediments that supported the model-based assumption of ion mobility as the controlling factor when comparing the electrochemical polarization of different cations (e.g., Ben Moshe et al. (2021), Hao et al. (2015), and Vaudelet et al. (2011)). Ben Moshe et al., 2021 investigated the suitability of SIP as a monitoring tool in breakthrough-curve analysis under cation exchange conditions in mineral soils. They showed that the real part σ' can serve as a proxy for conservative transport but were not successful in explaining the dynamics of σ'' during cation exchange or combining them with a reactive-transport model.

SIP surveys have been shown to be sensitive to the presence of solid (i.e., particulate) OM in sediments, with the signal strength of SIP being proportional to the cation exchange capacity (CEC) of OM (Strobel, Doerrich, et al., 2023). However, it is still up for debate whether electrochemical polarization in OM is similar to that at mineral surfaces or whether other factors such as the 3D-structure of OM and organo-mineral complexes yield different polarization mechanisms than those on inorganic minerals (Katona et al., 2021; Mellage, Zakai, et al., 2022; Schwartz & Furman, 2014). Measurements of σ'' are inherently non-selective and depend on a multitude of factors that are often coupled, integrating parallel contributions from different components of a porous medium. One major difficulty is therefore to distinguish between parallel signal contributions when

interpreting σ" changes. In particular, the electrical conductivity of the pore fluid (EC) often changes when investigating dynamic systems. It is often not feasible nor realistic to keep the EC constant during an experiment. Because the bulk fluid composition and EC can exert a significant control on σ" (Weller et al., 2011), changes in EC can mask σ" variations that are due to a difference in the EDL composition, hampering the interpretation of target processes from σ" signals (Mellage, Dörrich, et al., 2022).

In this study we focus on cation-exchange reactions on OM. We compare the SIP response during the injection of a monovalent cation (Na^+) and two divalent cations with different surface complexation strengths (Ca^{2+} and Zn^{2+}) into columns filled with a mixture of calcite sand and peat, and initially been loaded with Ca^{2+}-dominated pore water. With this work we want to test the following hypotheses:

1. Our understanding of surface polarization that was originally developed for mineral surfaces can also explain polarization on OM. Hence, a change in ion mobility on the surface is reflected in an increasing (e.g., via Na^+) or decreasing (e.g., via Zn^{2+}) imaginary conductivity.
2. We can qualitatively interpret the SIP data in the absence of a reactive-transport model or geochemical data to gain insights into the reaction dynamics. The breakthrough of the injected cation is distinguishable from the breakthrough of the conservatively behaving anion.
3. SIP measurements can be incorporated into a transport model accounting for competitive sorption to constrain the sorbing-phase concentration of the injected (or replaced) cation, thus improving model quality.

Finally, we provide an outlook on what is needed to successfully monitor reactions using SIP by non-geophysicists to unravel its potential in providing a glimpse into the "black box" of the subsurface without soil sampling.

2. Methods

2.1. Set-Up of Flow-Through Columns

For the flow-through experiments, we packed a total of four columns and conducted the experiments at room temperature (20.5°C). Two columns were packed with a mixture of calcite (marble) sand and 20% (w/w) solid OM (called OM01 and OM02) and the other two were packed with pure calcite (marble) sand (S01 and S02) serving as the OM-free control. The TOC content of OM01 and OM02 was 2.9%. We used the same columns, tubing, pumps and wet-packing procedure as Strobel, Doerrich, et al., 2023. Figure 1 shows an overview of the experimental setup and the different injection phases. Prior to packing, the marble sand was sieved to obtain a grain size distribution between 70 µm–2 mm, washed with deionized water and submerged in a $CaCl_2$ bath (5 mmol L^{-1}) for 36 hr to saturate charged surfaces with Ca^{2+} ions. The sand was then rinsed with $CaCl_2$ solution and dried at 70°C, overnight. Targeting the application of SIP to monitor cation exchange in groundwater systems, we used a natural OM sampled from the peat layer of the Ammer floodplain aquifer, near Tübingen Germany, as the OM. The peat, described in detail in a previous study (Strobel, Doerrich, et al., 2023), was dried at 30°C in a drying oven and homogenized after the removal of larger woody debris (>2 mm). Once packed, we sealed the columns for 4 weeks, for a static (no-flow) period, before starting the equilibration of the columns with pore water by pumping groundwater at a flow rate of 12 mL hr^{-1} (2.2 cm hr^{-1}) for 72 hr (corresponding to 8.7 pore volumes) to ensure equal EC at the inlet and outlet prior to tracer injection. Groundwater from the same aquifer from which we obtained the peat, was pumped directly in the field into air-tight bags (Tedlar®, Sigma Aldrich) and stored at 10°C (mean groundwater temperature) prior to use. Before injection, the groundwater was equilibrated to reach room temperature (20°C) over 24 hr.

Following the equilibration, we injected 8.8 mM of NaBr during a 72 hr pulse followed by a shift to pure groundwater for the subsequent 72 hr. The set-up of the injection, combining a syringe pump for spiking and a main line connected to a peristaltic pump, is described in detail by Strobel, Abramov, et al., 2023. Briefly, we set a pumping rate of 0.2 mL hr^{-1} at the syringe pump for spiking the inflow with NaBr, and 12 mL hr^{-1} at the peristaltic pump. This guaranteed mixing of the inflow solution at the desired concentration. The subsequent injections of 8 mM $CaBr_2$ and 10.2 mM $ZnBr_2$ were injected over 48 hr pulses followed by 48 hr of pure groundwater, without varying the flow rates. We collected outflow samples every hour for the first 12 hr of each pulse injection, followed by 2–3 samples per day in the following days, followed by hourly samples after the shift to clean groundwater, corresponding to the desorption front. The inflow was sampled right before starting the injection and at the end of each injection.

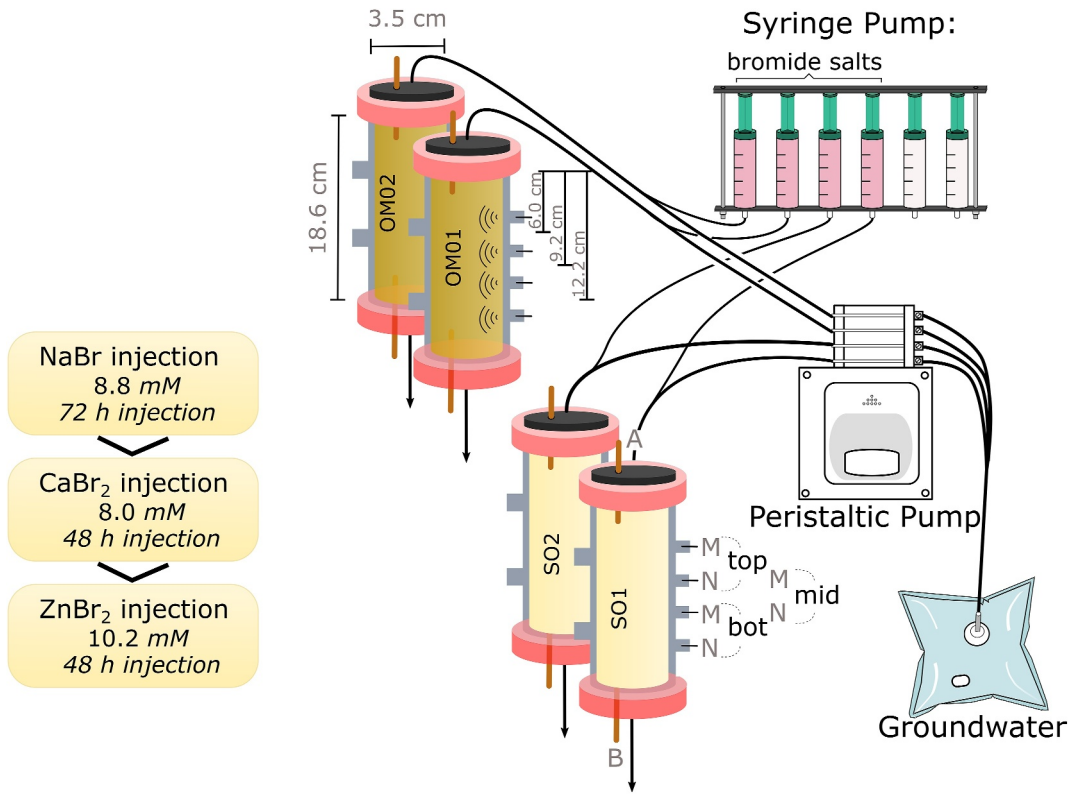

Figure 1. Schematic overview of the experimental set-up. Duplicate columns of sand only (S01 & S02) and sand with 20% (w/w) solid organic matter (OM01 & OM02) were equipped with four potential electrodes (called M & N) along the flow path and two current electrodes (called A & B) at the top and bottom caps. The inflowing solution consisted of natural groundwater to which the bromide salts were added directly before the inlet using a syringe pump. Flow is from top to bottom.

2.2. Sample Analysis

We analyzed samples for pH and EC immediately after sample collection using handheld pH and EC electrodes (LAQUAtwin® EC-22 and pH-11, HORIBA Scientific). The samples were then acidified (HNO_3) for cation analysis. Major anions and cations were quantified using ion chromatography (Metrohm, Germany). Zinc was measured using MP-AES (4200 MP-AES, Agilent Technologies, Australia, 213.857 nm). At the end of the experiment, we sampled the solid matrix by homogenizing the sediment of each column and measured the CEC of the homogeneous mixture in triplicates using the ammonium-acetate method as previously described by Strobel, Doerrich, et al., 2023.

2.3. SIP Measurements

Phase shift (-φ) and impedance magnitude (|Z|) were recorded over 41 log-frequency intervals between 0.1 and 1,000 Hz using a reference resistor of 100 Ω and an amplitude of 5 V (Portable SIP Unit, Ontash & Ermac Inc., USA). The results were converted to apparent frequency-dependent complex conductivities using a geometric factor, k [m], that was experimentally determined via measurements of the apparent EC of the columns filled with water of known conductivity. SIP measurements were performed at three locations using the upper, middle, and lower potential-electrode pairs (see Figure 1). SIP measurements were performed every 30 min to 1 hr on all three potential electrode channels. For the time-series analysis, the change in complex conductivity after $t = 0$ hr was monitored at a frequency of 1 Hz. We chose this frequency as it exhibits no impact of high frequency noise. Choosing a different frequency would yield similar results, but with a different absolute magnitude.

2.4. Cation-Exchange and Transport Model

We simulated the cation exchange between Na^+-Me^{2+}, Ca^{2+}-Mg^{2+}, and Zn^{2+}-Me^{2+} as competitive Langmuir sorption onto the OM. We combined the major background ions, Ca^{2+} and Mg^{2+}, into one species, Me^{2+}, for the model due to their similar ion exchange behavior, as done previously in Strobel, Abramov, et al. (2023). We assume that the sorption rate of cation i is proportional to the concentration of free sorption sites s_{free} (mmol g^{-1}) and to the aqueous cation concentration, c_i (mmol L^{-1}).

$$r^i_{\text{sorb}} = k^i_{\text{sorb}} \cdot c_i \cdot s_{\text{free}} \tag{1}$$

For desorption, we use a first-order rate law dependent on the sorbed cation concentration s_i (mmol g^{-1}).

$$r^i_{\text{desorb}} = k^i_{\text{desorb}} \cdot s_i \tag{2}$$

To reduce the number of parameters, we parameterized the rate constants as follows. We set $k_{\text{sorb},i} = \frac{k_{\text{desorb},i}}{K_i}$, where K_i (mmol L^{-1}) is the half-saturation constant of sorption, or the inverse of the equilibrium constant. We use the same $k_{\text{desorb},i}$ (s^{-1}) for Na^+ and Ca^{2+}, but allow the rate constant to differ for Zn^{2+}, which forms stronger surface complexes. In the limit of $k_{\text{desorb}} \to \infty$, this formulation of kinetic sorption is mechanistically equivalent to competitive Langmuir sorption at equilibrium. Assuming that the total charge on sorption sites is limited to $s_{\max}$ (mmol g^{-1}), the concentration of free sorption sites s_{free} is given by:

$$s_{\text{free}} = s_{\max} - \sum_{j=1}^{N} z_j \cdot s_j \tag{3}$$

where z_j is the charge of cation j, and N is the number of species. This yields the following equations for the sorbed and aqueous concentration of cation i:

$$\frac{\partial s_i}{\partial t} = r^i_{\text{sorb}} - r^i_{\text{desorb}} \tag{4}$$

$$\frac{\partial c_i}{\partial t} + v\frac{\partial c_i}{\partial x} - D\frac{\partial^2 c_i}{\partial x^2} = \frac{\rho_b}{n_e}\left(r^i_{\text{desorb}} - r^i_{\text{sorb}}\right) \tag{5}$$

in which, t and x denote the temporal and spatial coordinates, n_e (−) and ρ_b (g L^{-1}) are the effective porosity and bulk density, respectively, v (m s^{-1}) is the effective linear velocity. We computed the bulk density based on the solid density by $\rho_b = (1 - n_e)\rho_s$. The solid density ρ_s was estimated as 2.46 g cm^{-3} following Rühlmann et al. (2006) to account for the lower density of the OM. D (m^2 s^{-1}) is the dispersion coefficient, calculated from the pore diffusion coefficient D_p (m^2 s^{-1}) of each dissolved ion and the dispersivity α (m) of the OM-sand mix, using the approach of Scheidegger (1961): $D = D_p + \alpha v$. For the Zn^{2+} injection experiment, we consider the precipitation of zinc carbonate (Patterson et al., 1977) as a first-order reaction:

$$r_{\text{precip}} = -k_{\text{precip}} \cdot c_{Zn^{2+}} \tag{6}$$

with the rate constant k_{precip} [s^{-1}]. Equation 6 was added to the term in brackets on the right-hand side of Equation 5 for the Zn^{2+} case.

The initial conditions were based on the assumption that aqueous and sorbed concentrations are at equilibrium. Using the known composition of the injected groundwater for solute concentrations, we computed the initial sorbed concentrations $s_{0,i}$ as follows:

$$s_{0,i} = s_{\max}\frac{c_i}{K_i\left(1 + \sum_{j=1}^{N} z_j \frac{c_j}{K_j}\right)} \tag{7}$$

At the inflow boundary, we fixed the concentrations to the values in the inflow solution. At the outflow boundary, we assumed the dispersive flux to be zero and considered only the advective transport out of the column.

We discretized Equations 4 and 5, which describe transport and reactions in the column, using a finite volume approach. The system of ordinary differential equations obtained from discretization was solved using a Backwards Differentiation Formula (Byrne & Hindmarsh, 1975; Jackson & Sacks-Davis, 1980) using the Python library Sunode (Seyboldt et al., 2024) which wraps the CVODES module of the SUNDIALS library (Hindmarsh et al., 2005; Serban & Hindmarsh, 2008).

2.4.1. Implementing $\Delta\sigma''$ as a Proxy for the Sorbing-Phase Concentrations

For the parameter estimation we combined knowledge of the aqueous phase concentrations at the outflow with knowledge of the change in sorbed concentrations as inferred from $\Delta\sigma''$, the change in imaginary conductivity. To directly compare the simulated sorbed concentrations to $\Delta\sigma''$, we assume that $\Delta\sigma''$ can be decomposed into contributions of the ion exchange in the EDL, $\Delta\sigma''_{\mathrm{IE}}$ (μS cm^{-1}), and the ionic strength of the bulk fluid to the change in polarization, $\Delta\sigma''_{\mathrm{EC}}$ (μS cm^{-1}):

$$\Delta\sigma'' = \Delta\sigma''_{\mathrm{IE}} + \Delta\sigma''_{\mathrm{EC}} = \Delta\sigma''_{\mathrm{IE}} + a \cdot c_{\mathrm{Br^-}} \tag{8}$$

In which a (μS L cm^{-1} mmol^{-1}) is the linear proportionality constant between the aqueous concentration of bromide $c_{\mathrm{Br^-}}$ (mmol L^{-1}) at the midpoint of the potential electrode pair and $\Delta\sigma''_{\mathrm{EC}}$. This approach is based on the assumptions that (a) c_{Br^-} is a proxy for the change in EC and (b) that the relationship is linear. Weller et al. (2011) found a power law relationship with an exponent of around 0.5 between salinity and the imaginary conductivity in sandstone samples. In our experiments the EC ranged from 800 to 2,600 μS cm^{-1}, a much narrower range than the 250 to $23{\cdot}10^3$ μS cm^{-1} used by Weller et al. (2011) so we decided to assume the simplest possible, linear relationship. In experimental phases where we did not expect major changes in the chemical composition of the EDL while the EC was changing, we observed a satisfactory linear relationship between $c_{\mathrm{Br^-}}$ and $\Delta\sigma''$ (see Figure S1 in Supporting Information S1) making us confident that this is a good first approximation of this clearly more complex relationship.

Secondly, we estimated a compound-specific proportionality constant p_{inj} (μS g cm^{-1} mmol^{-1}) between the sorbed concentration of the injected cation and $\Delta\sigma''_{\mathrm{IE}}$ that enabled a direct link between $\Delta\sigma''_{\mathrm{IE}}$ and the resulting sorbed concentration s_{inj} (mmol g$^{-1}{}_{\mathrm{sed}}$) at the midpoint of the electrode pair:

$$\Delta\sigma''_{\mathrm{IE}} = p_{\mathrm{inj}} \cdot s_{\mathrm{inj}} \tag{9}$$

2.4.2. Parameter Inference by the Markov Chain Monte Carlo Method

We estimated parameters using a Bayesian approach, which yields parameter distributions rather than single values to account for uncertainty. This approach requires defining prior distributions of the parameter values that represent expert knowledge about reasonable parameter ranges. These distributions are then updated with a likelihood function which can be interpreted as a goodness-of-fit measure of the model to the data. The resulting posterior distribution represents the remaining uncertainty in the parameters after the model has been fitted to the data.

Parameters that were set to fixed values in the simulation are shown in Table S1 in Supporting Information S1. We defined prior distributions based on physical constraints, literature values, and order-of-magnitude estimates (see Table S2 in Supporting Information S1). For the likelihood, we used concentration time series of injected and background ions (c_{inj} and c_{bg}) at the column outflow, and $\Delta\sigma''$ at the three SIP measurement locations. We assumed that the data are normally distributed around the simulated values, with a fixed standard deviation per data type.

We sampled the posterior distribution with a Sequential Monte Carlo (SMC) algorithm using the Python package PyMC (Abril-Pla et al., 2023). We generated 2,000 posterior samples in 4 independent chains (i.e., 500 samples per chain). To assess convergence, we computed the $\hat{R}$ -criterion (Vehtari et al., 2021) using the ArViz library (Kumar et al., 2019).

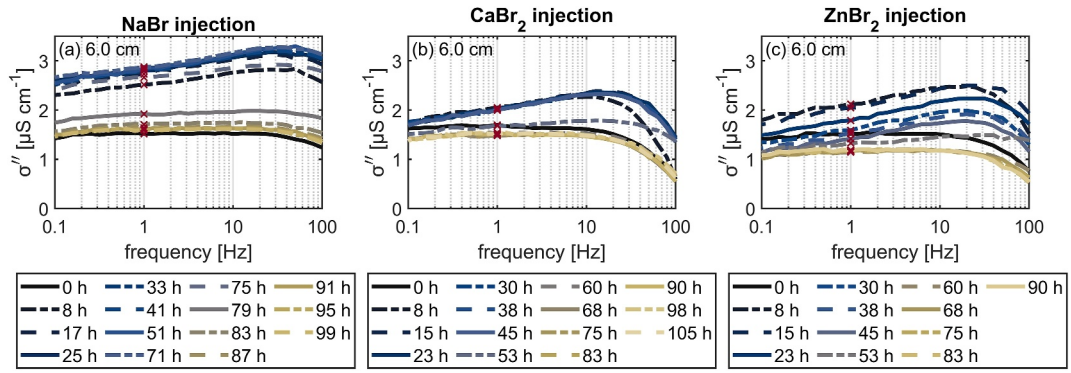

Figure 2. Selected imaginary conductivity (σ'') spectra during the (a) Na^+-, (b) Ca^{2+}- and (c) Zn^{2+}-injection experiments at the spectral induced polarization measurement location closest to the inlet (6 cm) in column OM01. (Note: Na^+ was injected for 72 hr whereas Ca^{2+} and Zn^{2+} for 48 hr). The red crosses mark the measurements at 1 Hz, presented henceforth for time-series analysis. The spectra are truncated at 100 Hz due to noise at higher frequencies.

3. Results and Discussion

Figure 2 shows σ'' spectra measured at 6 cm from the inlet at selected time points for all three cation-injection experiments (Na^+, Ca^{2+} and Zn^{2+}) in the OM-containing treatment. (Note: all spectra are shown in Figures S2 and S3 in Supporting Information S1). The spectra show a gradual increase from low to higher frequency reaching a peak above 10 Hz. Since the spectral characteristics were similar across all experiments we conclude that a similar type of polarization (and thus reaction) process took place in all experiments. The lack of frequency-dependent changes of σ'' suggests that this process affects a wide range of polarization length scales, as can be expected from cation exchange on a heterogeneous matrix as OM. In the pure-sand control columns, σ'' was close to the detection limit and did not change over time in all experiments (see Figures S4 and S5 in Supporting Information S1), indicating the absence of appreciable cation exchange. This was fully confirmed by the outflow concentration data for the NaBr and $CaBr_2$ injection (see Figures S8 and S9 in Supporting Information S1). For the $ZnBr_2$ injection we observe some evidence for cation exchange also in the pure sand columns which is however much faster and lower in magnitude compared to the OM containing columns (data are shown and discussed in Section 3.2 in detail). Therefore, we focus in the following on a time-series analysis of the OM-containing column, and present σ'' values at the single frequency of 1 Hz (highlighted by red crosses in Figure 2). We chose that frequency to avoid any effects of measurement noise at higher frequencies. Both OM-containing columns showed a generally similar behavior. However, the data set in OM02 was interrupted by unwanted peaks of high salt concentration, caused by errors when changing the syringe pump. Thus, we focus our time-series analysis on OM01 but present all data of OM02 in the supporting information (Figures S6 and S10 in Supporting Information S1).

3.1. Qualitative Interpretation of SIP Data

In Figure 3 we compare the change in real and imaginary conductivity as gray, dashed lines and colored lines, respectively, in column OM01. The corresponding phase shifts and impedances are shown in Figure S7 in Supporting Information S1. Columns of subplots represent experiments with different cation injections, rows of subplots represent different locations of SIP measurements, that is, with increasing distance from the inlet. For a direct comparison across potential electrode pairs (6, 9.2 and 12.2 cm) and experiments, the axes limits are held constant in all panels and signals are plotted as the difference, Δ, between measurement and the baseline prior to cation injection. The arrival time, and pulse duration of the conservative anion, Br^-, is captured by $\Delta\sigma'$ (Ben Moshe et al., 2021; Strobel, Abramov, et al., 2023) in all cases. The increase in $\Delta\sigma'$ was the lowest during the NaBr injection, owing to the Na-Br mole ratio, yielding only half of the bromide concentration injected during the $CaBr_2$ and $ZnBr_2$ injections (injected cation concentration in all cases: 8–10 mmol L^{-1}).

The major background cations in the pore water were Ca^{2+} and Mg^{2+}, at 3.45 and 1.75 mmol L^{-1}, respectively. Owing to their similar hydrated radii (412 and 428 p.m. (Amelung et al., 2018)), valence and complexation capabilities, that in turn yield similar ion mobilities (Revil et al., 1998) in the EDL, we did not expect a strong effect of Ca^{2+}-Mg^{2+} exchange on σ''. The $CaBr_2$ injection (Figures 3d–3f), therefore, served as the injection

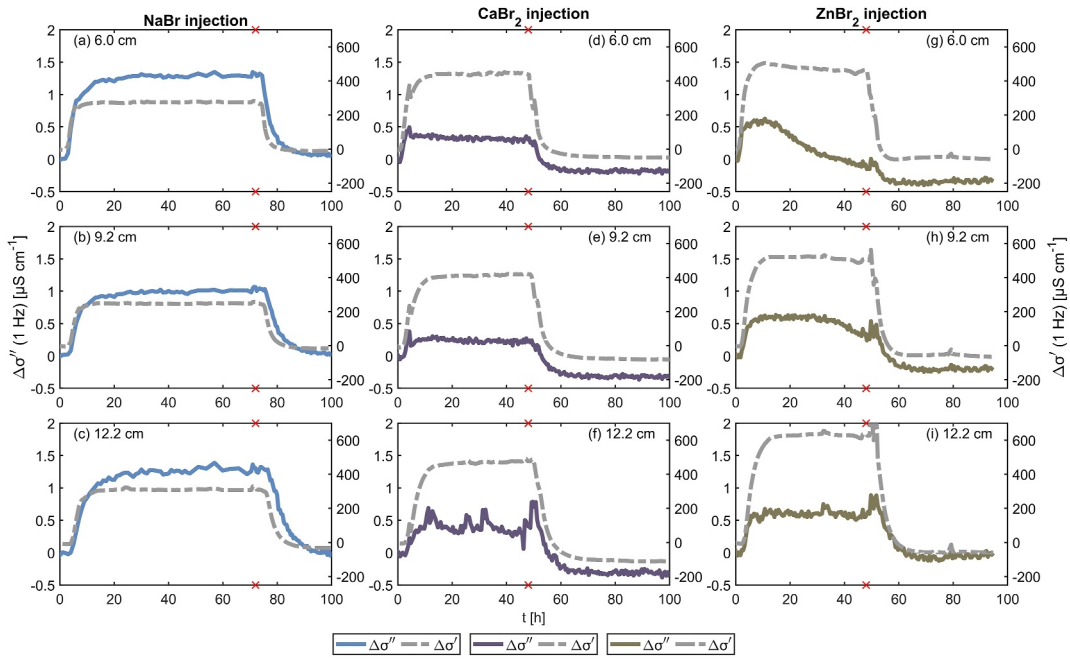

Figure 3. Comparison of the change (Δ) in real ($\Delta\sigma'$) and imaginary conductivity ($\Delta\sigma''$), at 1 Hz, during all three cation injections: NaBr (a–c), $CaBr_2$ (d–f) and $ZnBr_2$ (g–i). Red crosses on the *x*-axis mark the end of each injection, where NaBr, $CaBr_2$, $ZnBr_2$ were injected for 72, 48 and 48 hr, respectively. Subplot rows depict all three SIP-measurement locations shown here for column OM01, where the distance corresponds to the midpoint of the potential electrode pair relative to the inlet.

pulse during which EC effects dominate over changes in the EDL composition. In agreement with our expectation, the $\Delta\sigma''$ for the $CaBr_2$ injection is the lowest of all three cation-injection experiments and across all locations of SIP measurements.

During the NaBr injection (Figures 3a–3c), $\Delta\sigma''$ increased up to 1–1.4 μS cm^{-1} (depending on the SIP location) and stayed constant at its maximum value until the NaBr was stopped after 72 hr and σ'' dropped again to the initial value (i.e., $\Delta\sigma'' = 0$). The increase in polarization is driven by the higher concentration of more mobile Na^+ ions in the EDL, relative to the lower mobility background divalent cations. The separate conduction and polarization controls on σ' and σ'', respectively, become particularly evident at 12.2 cm where a time-lag can be observed between the increase and decrease of $\Delta\sigma'$ and $\Delta\sigma''$. The time delay points to the retention (i.e., sorption or ion-exchange) of Na^+ in the matrix relative to the conservative transport of Br^- at the flow velocity. Moreover, the maximum $\Delta\sigma''$ is about four times higher than during the $CaBr_2$ injection. Both the retarded $\Delta\sigma''$-front and the maximum $\Delta\sigma''$ support our hypothesis that a significant fraction of Na^+ exchanged Ca^{2+} and Mg^{2+} in the OM-sand matrix, similar to previously reported findings by (Strobel, Abramov, et al., 2023).

The $ZnBr_2$ injection (Figures 3g–3i), yielded a spatially variant trend in the SIP measurements. At all locations, there was an increase in $\Delta\sigma'$ and $\Delta\sigma''$ as a result of the $ZnBr_2$ injection and a decrease in $\Delta\sigma'$ and $\Delta\sigma''$ once the injection was stopped. However, unlike the plateau that developed during the Na^+ and Ca^{2+} injections, the $ZnBr_2$ injection led to a drop in $\Delta\sigma''$ at 6 cm (Figure 3g) following the initial increase (at 10 hr), from +0.6 μS cm^{-1} to −0.15 μS cm^{-1}, despite the fact that Zn^{2+} was continuously injected for 48 hr. Similarly (but delayed), at 9.2 cm from the inlet (Figure 3h), $\Delta\sigma''$ stayed constant at +0.6 μS cm^{-1} until 34 hr, followed by a decrease to 0.25 μS cm^{-1} at 48 hr, whereas no decrease at all was observed at 12.2 cm. The different temporal trends are directly evident when comparing the $ZnBr_2$ with the $CaBr_2$ case and agree with our hypothesis that exchange of Ca^{2+}/Mg^{2+} ions by the more strongly complexing Zn^{2+} ions results in a decrease of σ''. The fact that we observe the strongest decrease of $\Delta\sigma''$ closest to the inlet and no decrease at 12.2 cm suggests that Zn^{2+} ions were completely sorbed in the upper half of the column, agreeing well with the fact that we did not detect any Zn^{2+} breakthrough at the outlet (see details below). After the stop of the injection, $\Delta\sigma''$ stabilized at −0.1 μS cm^{-1} (12.2 cm) to −0.35 μS cm^{-1} (6 cm), highlighting that the pre-injection equilibrium was not reached within the time of the experiment

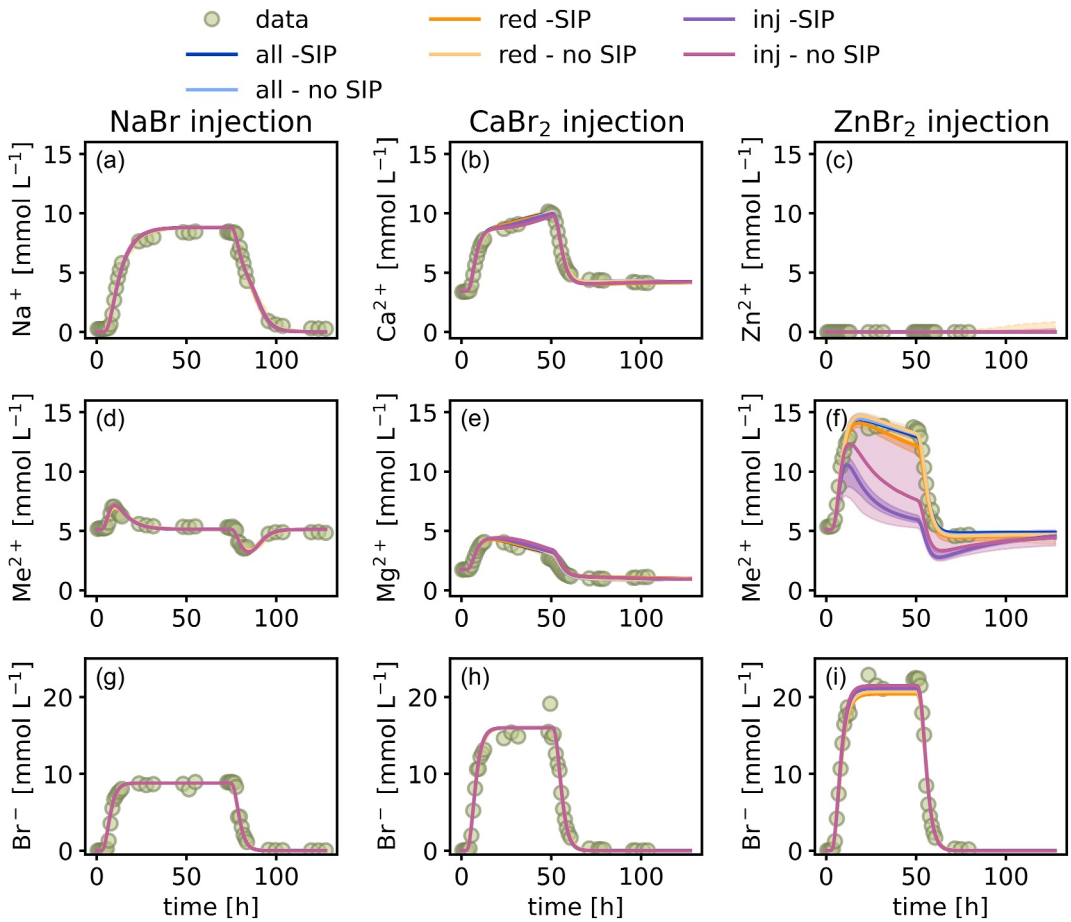

Figure 4. Simulated concentrations at the column outlet of injected cations (a–c), the corresponding background or competing cations (d–f) and the conservative anion Br^- (g–i) for the three different injections. During the NaBr and $ZnBr_2$ injections Mg^{2+} and Ca^{2+}concentrations are lumped as Me^{2+}, whereas in the CaBr injection, Mg^{2+} is the sole competing ion and is shown individually. Six modeling scenarios are compared that rely on varying amounts of data for parameter estimation: all concentration data with or without spectral induced polarization (SIP) (all-SIP or -no SIP), every 3rd concentration data point with or without SIP (red-SIP or -no SIP), only the injected cation concentrations with or without SIP (inj-SIP or -no SIP). The different parameter estimation scenarios fall on top of each other in the Na^+ and Ca^{2+}experiments, and differences are only discernible in panels (f) and (i). The shaded areas show the range between the 5th and 95th quantile of the fit.

and that the difference in EDL composition is highest close to the inlet where the Zn^{2+} was sorbed. This suggests that the desorption of Zn^{2+} was considerably slower than its adsorption.

3.2. Coupling Concentration and $\Delta\sigma''$-Data

The concentration measurements at the column outlet confirm the qualitative interpretation of $\Delta\sigma''$ discussed in the previous section. In Figure 4, the concentrations of the injected cations, the background cations, and of the conservatively behaving anion, Br^-, are shown for all three injection experiments. When presenting the NaBr- and $ZnBr_2$-injection, we combine the concentrations of Ca^{2+} and Mg^{2+} into a single species, Me^{2+}, as they show a very similar behavior (Figures 4d and 4f). Only in the case of the Ca^{2+}-injection we distinguish the two species, because in this case their slightly different sorption behavior becomes relevant (Figures 4b and 4e). Cation exchange is evident in all three injection experiments via the measured increase in the concentration of the background ion (Me^{2+} for Na^+ and Zn^{2+} and Mg^{2+} for Ca^{2+}) during breakthrough of the injection front (Figures 4d–4f). In the NaBr-injection experiment, ion exchange reaches equilibrium across the entire columns with Na^+- and Me^{2+}-concentrations both reaching the inflow concentration at the outlet (Figures 4a and 4d). Conversely, for $CaBr_2$ and $ZnBr_2$ this is not the case. As already postulated based on the $\Delta\sigma''$ data, the sorption of Zn^{2+} onto OM

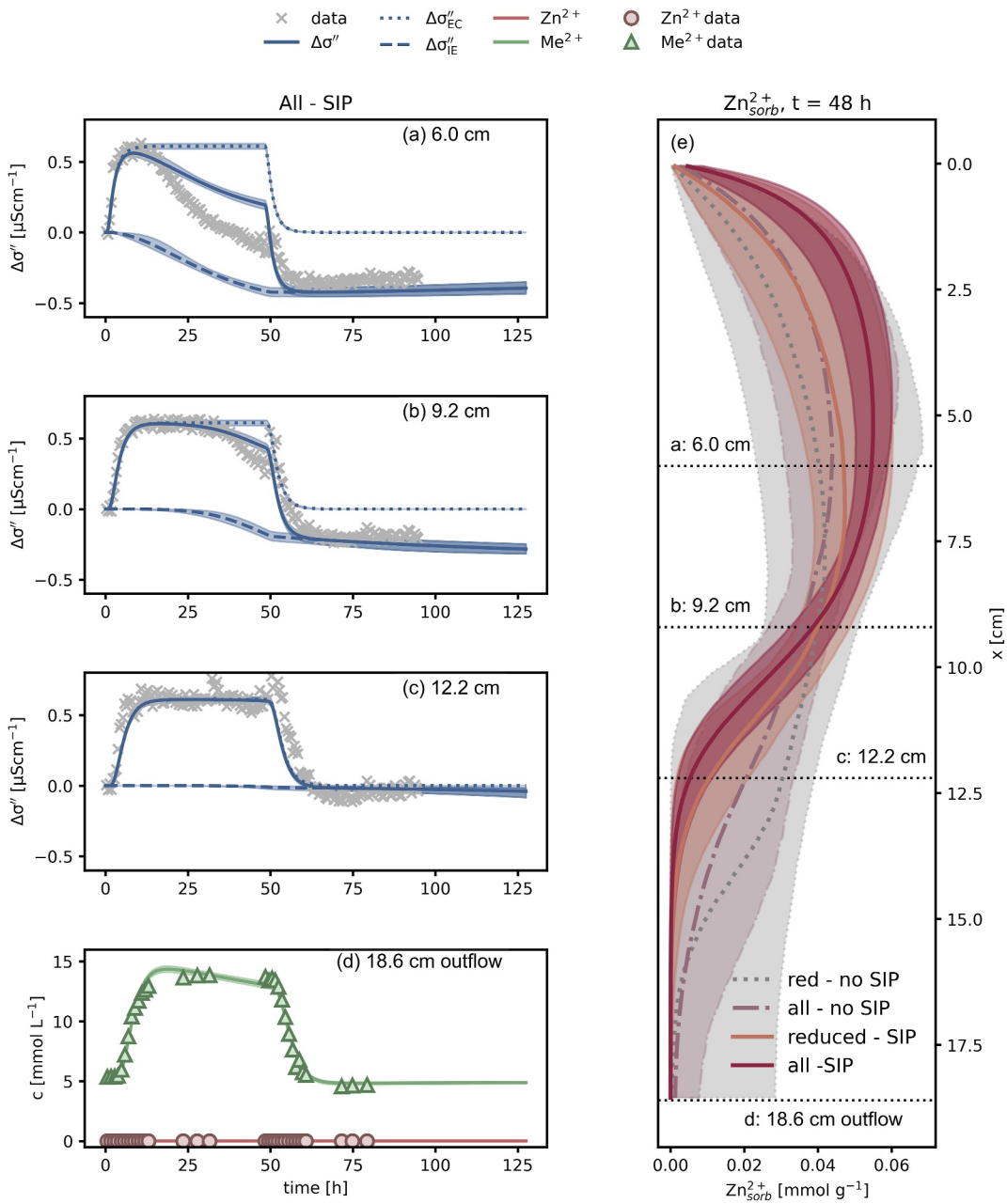

Figure 5. Model-data comparison of the simulation of the Zn^{2+}-experiment using all geochemical data, all-SIP (left panels). Panels (a–c) show the simulated change (Δ) in imaginary conductivity ($\Delta\sigma''$) compared to measured $\Delta\sigma''$ at all spectral induced polarization (SIP) measurement locations. In addition, the contribution of electrical conductivity, $\Delta\sigma''_{EC}$, and ion exchange, $\Delta\sigma''_{IE}$, to the overall change in σ'' are shown separately as dotted and dashed lines, respectively. Panel (d) compares simulated versus measured concentrations. Simulated sorbed concentration profiles of Zn^{2+} at the end of the experiment are shown for selected parameter estimation scenarios (e). The dashed lines in the panel denote the location of the SIP measurements and the outflow and the shaded areas show the range between the 5th and 95th quantile.

is stronger than that of Me^{2+}, and thus prevents its breakthrough at the outlet (Figure 4c), yielding a strong release of background Me^{2+}-ions (Figure 4f). For $CaBr_2$, the very similar sorption strengths of Ca^{2+} and Mg^{2+} result in a quick local reequilibration that is only changing gradually.

We simulated the transport and ion exchange reaction to confirm our interpretation of the reactive processes. By incorporating the $\Delta\sigma''$ data into the parameter estimation scheme, as a proxy for the sorbed concentration of the injected cation, we investigate the potential additional information that can be gained from measuring SIP

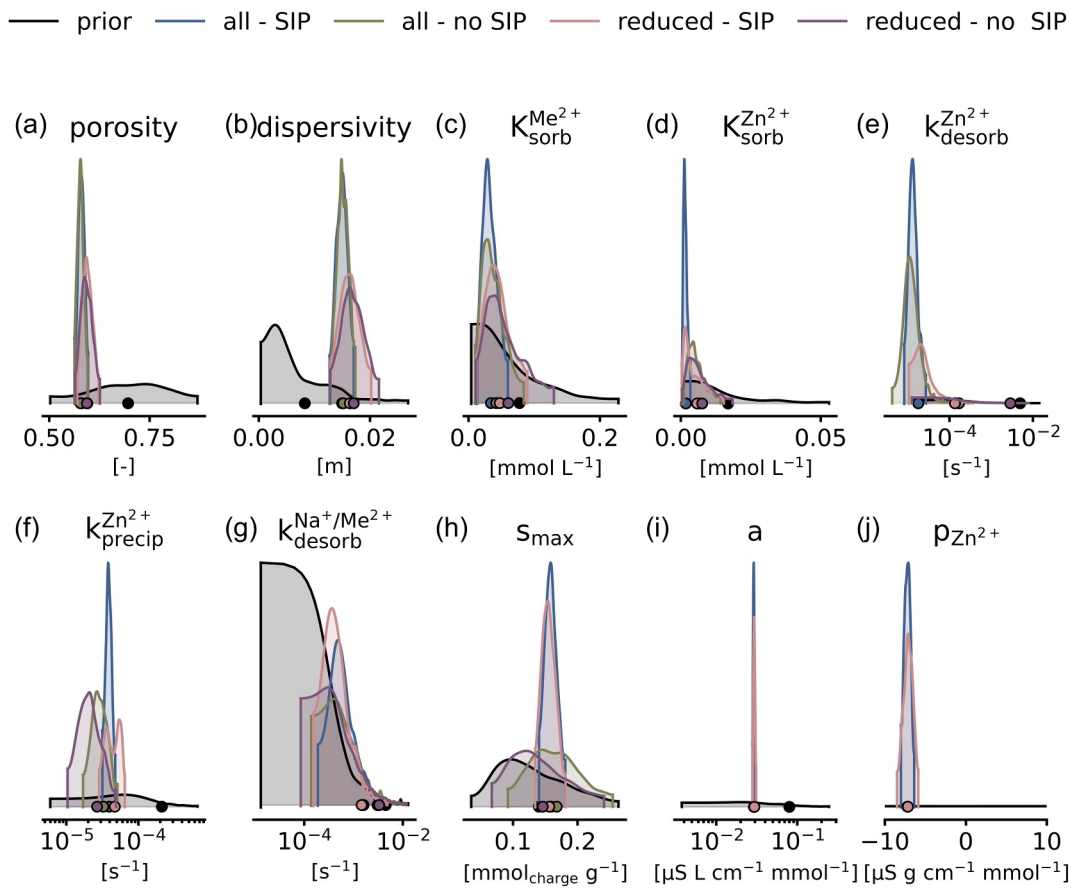

Figure 6. Kernel density estimates of the prior and posterior distributions of parameters relevant for the Zn^{2+} experiment. The posterior distributions are shown for the different scenarios of all concentration data or a reduced data set of every 3rd datapoint with or without Spectral induced polarization data. Plots are cut at the 94% highest density interval.

alongside geochemical sampling schemes. We estimated the parameters six times based on a combination of three different data sets of concentration data either with or without the SIP data as additional information: Using all available data (all—SIP and all—no SIP), using every 3rd concentration data point and the SIP data (red—SIP and red—no SIP) or using only the concentration time series of the injected cation (inj—SIP and inj—no SIP). The resulting fits of the six scenarios are shown alongside with the data in Figure 4. The results show that our model can accurately predict both conservative transport (Figures 4g–4i) and the cation-exchange processes in the NaBr- and $CaBr_2$-injection experiments (Figures 4a, 4b, 4d, and 4e) with only minor variations between the different scenarios. In these cases, the concentration time series of the injected cation in the outlet or using only a subset of the data were sufficient to constrain the model, and the addition of SIP measurements did not improve the calibration outcome. It is noteworthy, that the inclusion of the SIP data slightly reduces the parameter uncertainty of the sorption parameters $K_{Zn,\ sorb}$ and $K_{Me,\ sorb}$ (see Figure 6 and Figures S12–S14 in Supporting Information S1).

However, in the $ZnBr_2$-injection experiment, we observe a major difference between the calibration scenarios, with and without the concentration data of the background cation. Because Zn^{2+} did not break through during the experiment, the Zn^{2+} time-series does not provide sufficient information to constrain the model and accurately predict the Me^{2+}-concentrations (Figure 4f, pink line), which is also highlighted in the high uncertainty of the model fit when using only the Zn^{2+} data (shown by the shaded pink area). Adding information about the sorbing-phase concentrations by incorporating the SIP data reduces the model uncertainty, but does not improve the fit (Figure 4f, purple line & area). We speculate that the formulation of our ion-exchange model or the linear proportionality between the sorbing-phase concentration and $\Delta\sigma''$ does not fully capture the processes relevant for the complexation of Zn^{2+}. Zn^{2+} is a heavy-metal ion that interacts differently with charged surfaces than the

ions of the alkaline (earth) metals Na^+, Ca^{2+}, and Mg^{2+} (Amelung et al., 2018; Himes & Barber, 1957; Randhawa & Broadbent, 1965). It is therefore reasonable to expect that the reaction mechanism is not fully described by our 2nd-order formulation. This could also explain the difference of the simulated Me^{2+} concentrations (Figure 4f) when using all available data compared to the measurements. They exhibit an almost constant plateau, rather than showing a gradual decrease of the Me^{2+} concentrations as predicted by the model. In addition, we had to add a first-order precipitation term to the model to account for zinc-carbonate precipitation in the bicarbonate dominated groundwater in order to prevent the model from predicting a breakthrough of Zn^{2+}. This additional degree of freedom might not be constrained by our data even when adding the SIP data. In the absence of background concentration data (inj-SIP case), the model predicts an order of magnitude higher precipitation rates and consequently a much lower fraction of sorbed Zn^{2+} (see Figure S11 in Supporting Information S1) compared to the other scenarios. Finally, while in theory, the zinc carbonate precipitation could have also caused calcite dissolution, the excellent agreement of our model with the Zn^{2+} and Ca^{2+}/Me^{2+} concentration provides strong evidence to suggest that there was no additional source of Ca^{2+} ions. Moreover, the fact that we do not observe unexpectedly high Ca^{2+} concentrations in the control (marble sand only) columns (see Figures S8 and S9 in Supporting Information S1) further suggests that we included all relevant processes into our reactive transport model, and justify the omission of calcite dissolution.

In Figure 5 we show the model-data comparison for the outflow concentration measurements (d) alongside with the fit of the SIP data (a–c) for the scenario with all data used for parameter estimation. In addition, Figure 5e shows the simulated Zn^{2+} concentrations at the end of the ZnBr-injection for the all chemistry and reduced chemistry data case. The fit to the SIP data for the other scenarios and the corresponding profiles are shown in Figures S10 and S11 in Supporting Information S1, but differences in the fit to the SIP data between the scenarios are subtle. In the following, we compare the different parameter-estimation scenarios in more detail and focus our analysis on the $ZnBr_2$ injection, because of the spatial variability in the extent of the Zn^{2+} sorption inferred from our qualitative interpretation of the SIP data. The corresponding figures for the other two injection experiments are presented in Figures S8 and S9 in Supporting Information S1.

In all parameter-estimation scenarios the contribution of the EC to $\Delta\sigma''$ is similar and explains the initial increase of $\Delta\sigma''$ at all measurement locations. The model predicts a negative proportionality between sorbed Zn^{2+} concentration and $\Delta\sigma''$ that agrees with our hypothesis that the lower ion mobility of Zn^{2+} compared to Ca^{2+}/Mg^{2+} results in a decrease in σ''. The general temporal trends of the model agree with trends in the SIP data for both cases but underpredict the decrease of $\Delta\sigma''$ driven by Zn^{2+} sorption, in particular at 6.0 cm (Figure 5 a). A difference between the scenarios with and without SIP data lies in the position of the Zn^{2+} sorption front (Figure 5e) for both, the all chemistry and reduced chemistry scenario. With the information at the SIP electrodes, the uncertainty is considerably reduced and sorption is constrained to occur primarily before the 2nd electrode pair at 9.2 cm.

While all models yield similar model parameters (Figure 6), incorporating SIP data in the calibration scheme yields slightly lower parameter uncertainties. This highlights a potentially important additional information gained from its inclusion. Kernel density estimates of the posterior distributions of parameters not shown in Figure 6 are shown in Figures S15–S17 in Supporting Information S1 alongside with the mean parameter estimates of the "all-SIP" scenario in Table S3 in Supporting Information S1.

The linear $\Delta\sigma''$-$Zn^{2+}{}_{sorb}$ relationship we chose is probably an oversimplification of reality. Yet, it is striking how well this approach can reflect the general reaction trends. In our formulation, we neglect any effect of the zinc precipitate on the signal due to its low volume fraction and the generally high abundance of carbonates in the background solid matrix. In the upper section of the column (6.0 and 9.2 cm), where Zn^{2+}-sorption is taking place, however, the measured decrease in $\Delta\sigma''$ at the end of the $ZnBr_2$ injection (at around 50 hr), driven by the decrease in EC, is not as pronounced as predicted by the model nor measured during the corresponding increase at the onset of injection (0–10 hr). As this is only the case for the $ZnBr_2$ injection and does not happen in the other two experiments, we speculate that we still miss a process either in our conceptual model of induced polarization or the behavior of Zn^{2+} in this system.

4. Opportunities and Limitations for Reaction Monitoring With SIP

The present experiment exemplifies that SIP facilitates monitoring of reactions in the subsurface, but also highlights its limitations. The qualitative interpretation of complex-conductivity data is hampered by changes of EC modifying $\Delta\sigma''$. Thus, it can be advantageous to maintain constant EC or at least have phases of stable EC

during the reaction phase (Ben Moshe & Furman, 2022; Mellage, Zakai, et al., 2022). The approach outlined in this study accounts for EC changes, potentially extending the applicability of SIP to more dynamic systems. For instance, data from a (groundwater) tracer test could be utilized to calibrate the relationship between EC and $\Delta\sigma''$, which could then be applied to the main/target experiment. However, care must also be taken in the design of the tracer test, as the injection of a salt at high concentration will inevitably result in ion exchange. The qualitative interpretation of SIP data in dynamic systems requires a solid understanding of the relevant processes. Its complexity arises from the multitude of parameters that can affect the SIP signal and calls for the comprehensive monitoring of background chemistry (i.e., EC, pH, redox potential and concentration of major ions) during an experiment. The interpretation is further complicated by the absence of direct, quantitative links between geophysical measurements and geochemical parameters in such complex systems. Consequently, sufficient prior knowledge and experience is essential for effectively utilizing SIP in reaction monitoring.

The incorporation of SIP data into reactive-transport modeling schemes has been proposed (Kessouri et al., 2019), however the lack of petro-physical relationships that link specific processes to their σ'' signal is hampering its application. With the simple relationships in this work we demonstrate how quantitative coupling may be implemented. Yet, we acknowledge that the additional information gained, in most of our cases, was limited, and that the SIP data cannot fully replace concentration data of a reactive species. However, this is dependent on the target reactive process to be monitored and the availability of highly resolved concentration data. It is worth noting, that the incorporation of SIP data improved parameter estimation. Despite these limitations, the framework presented here demonstrates the potential for such integrated approaches and their applicability to various reactive scenarios. This coupling could lead to more accurate and comprehensive models, helped identifying missing processes and thereby advances our capability to monitor and interpret complex geochemical processes in situ.

5. Conclusions

The absence of changes in $\Delta\sigma''$ in the control columns without OM showed that electrochemical polarization is restricted to the OM in our system. The experiment was therefore suitable to examine whether the existing electrochemical polarization theory for mineral surfaces is also applicable to OM. The excellent agreement between our hypotheses on the effect of different cations on σ'' and the resulting $\Delta\sigma''$ (Figure 3) suggests that OM polarization qualtitatively follows similar principles as electrochemical polarization on mineral surfaces.

We were successful at monitoring conservative transport and cation exchange on OM through the interpretation of $\Delta\sigma''/\Delta\sigma'$-plots only. These plots condense information stemming from the multidimensional SIP measurements into a format that can be quickly evaluated and is thus valuable in the monitoring of column or other time-lapse experiments.

To do so, it is important to estimate the expected effect of a certain reaction on σ''. In this study, we focus on changes in the surface ion mobility of different cations in the EDL. This implies that during the reaction the surface charge density does not change dramatically. Quanitiative estimates of the surface ion mobility are often not available. Therefore, polarization models assume a fraction of the mobility in water (Revil et al., 1998; Vaudelet et al., 2011). This yields very similar ion mobilities and thus similar σ'' measurements should be expected for Ca^{2+} and Zn^{2+}, contradictory to our experimental results. The ion mobility in water is controlled primarily by the valence of the ion and its size and neglects any non-electrostatic interactions (e.g., surface-complexes) that can exist between the surface and the ion. Based on our experimental results and the resulting conceptual model we find it promising, from a geochemist's experimental perspective, to rely more on sorption coefficients to estimate ion mobilities for polarization models rather than relying on their diffusion coefficients in water. Sorption coefficients integrate all ion-surface interactions and can often be found in literature for different materials. In our experiment the estimated half-saturation concentrations or Langmuir-type sorption constants of the three cations differ by one order of magnitude (Figure 7), which agrees with the observed effects on σ''.

The experiment presented here is a proof-of-concept on how (S)IP data can be incorporated in reaction monitoring of reactions involving charged surfaces. The results of our reactive-transport model show how SIP data can quantitatively be coupled with geochemical data sets. Separating the changes in $\Delta\sigma''$ caused by changes in EC from those caused by the reaction can (a) enhance the interpretability of SIP signals in dynamic systems, (b) help

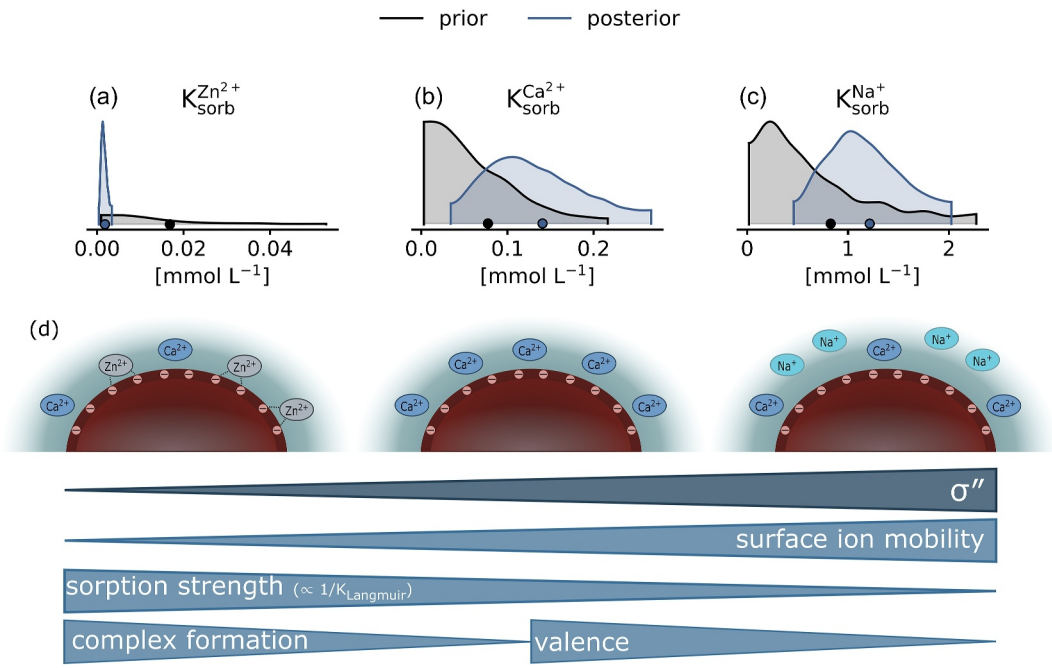

Figure 7. Prior and posterior kernel density distribution of the sorption half-saturation constants of the injected cations (a–c) of the scenario where all available data were used for parameter estimation. A schematic representation of the relationship between sorption of cations on organic matter and their respective effect on σ'' is shown in panel (d).

to identify overlooked processes, and (c) facilitate assessing the relative effect of different processes on σ'', in particular, through iterative steps between conceptual and mathematical modeling.

Data Availability Statement

The SIP data, the geochemical data and the Python codes for the reactive transport modeling are available at https://doi.org/10.5281/zenodo.12788754 under the MIT license (Strobel et al., 2024).

Acknowledgments
Adrian Mellage would like to acknowledge the financial support of the Baden-Württemberg Stiftung received for this project via the Eliteprogramme for Postdocs as well as the financial support of the Ministry for Science, Research and the Arts of Baden-Württemberg via the Research Seed Capital Program (RiSC). We thank Björn Spranglewski for his support with the IC measurements and Manuel Dörrich and Emma-Helen Stieff for help conducting the experiment. Open Access funding enabled and organized by Projekt DEAL. We are grateful to Matthias Bücker, two anonymous reviewers, and the Associate Editor, Lee Slater, whose constructive remarks have helped improve the paper.

References

Abril-Pla, O., Andreani, V., Carroll, C., Dong, L., Fonnesbeck, C. J., Kochurov, M., et al. (2023). PyMC: A modern, and comprehensive probabilistic programming framework in Python. *PeerJ Computer Science*, *9*, e1516. https://doi.org/10.7717/peerj-cs.1516

Albers, C. N., Banta, G. T., Hansen, P. E., & Jacobsen, O. S. (2009). The influence of organic matter on sorption and fate of glyphosate in soil – Comparing different soils and humic substances. *Environmental Pollution*, *157*(10), 2865–2870. https://doi.org/10.1016/j.envpol.2009.04.004

Amelung, W., Blume, H.-P., Fleige, H., Horn, R., Kandeler, E., Kögel-Knabner, I., et al. (2018). *Scheffer/Schachtschabel Lehrbuch der Bodenkunde (F. Scheffer & P. Schachtschabel, Trans.; 17., überarbeitete und ergänzte Auflage)*. Springer Berlin Heidelberg. https://doi.org/10.1007/978-3-662-55871-3

Atekwana, E. A., & Slater, L. D. (2009). Biogeophysics: A new Frontier in earth science research. *Reviews of Geophysics*, *47*(4), L12505. https://doi.org/10.1029/2009RG000285

Bate, B., Cao, J., Yang, Y., Cao, J., Zhang, C., & Zhang, S. (2023). Investigation of Cu adsorption and migration with spectral induced polarization in activated carbon. *Toxics*, *11*(3), 221. https://doi.org/10.3390/toxics11030221

Ben Moshe, S., & Furman, A. (2022). Real-time monitoring of organic contaminant adsorption in activated carbon filters using spectral induced polarization. *Water Research*, *212*, 118103. https://doi.org/10.1016/j.watres.2022.118103

Ben Moshe, S., Kessouri, P., Erlich, D., & Furman, A. (2021). Geophysically based analysis of breakthrough curves and ion exchange processes in soil. *Hydrology and Earth System Sciences*, *25*(6), 3041–3052. https://doi.org/10.5194/hess-25-3041-2021

Binley, A., & Slater, L. D. (2020). *Resistivity and induced polarization*. Cambridge University Press. https://doi.org/10.1017/9781108685955

Bücker, M., Flores Orozco, A., Undorf, S., & Kemna, A. (2019). On the role of stern- and diffuse-layer polarization mechanisms in porous media. *Journal of Geophysical Research: Solid Earth*, *124*(6), 5656–5677. https://doi.org/10.1029/2019JB017679

Byrne, G. D., & Hindmarsh, A. C. (1975). A polyalgorithm for the numerical solution of ordinary differential equations. *ACM Transactions on Mathematical Software*, *1*(1), 71–96. https://doi.org/10.1145/355626.355636

Flores Orozco, A., Williams, K. H., & Kemna, A. (2013). Time-lapse spectral induced polarization imaging of stimulated uranium bioremediation. *Near Surface Geophysics*, *11*(5), 531–544. https://doi.org/10.3997/1873-0604.2013020

Hao, N., Moysey, S. M. J., Powell, B. A., & Ntarlagiannis, D. (2015). Evaluation of surface sorption processes using spectral induced polarization and a (22)Na tracer. *Environmental Science & Technology*, *49*(16), 9866–9873. https://doi.org/10.1021/acs.est.5b01327

Himes, F. L., & Barber, S. A. (1957). Chelating ability of soil organic matter. *Soil Science Society of America Journal*, *21*(4), 368–373. https://doi.org/10.2136/sssaj1957.03615995002100040005x

Hindmarsh, A. C., Brown, P. N., Grant, K. E., Lee, S. L., Serban, R., Shumaker, D. E., & Woodward, C. S. (2005). Sundials: Suite of nonlinear and differential/algebraic equation solvers. *ACM Transactions on Mathematical Software*, *31*(3), 363–396. https://doi.org/10.1145/1089014.1089020

Huang, W., Peng, P., Yu, Z., & Fu, J. (2003). Effects of organic matter heterogeneity on sorption and desorption of organic contaminants by soils and sediments. *Applied Geochemistry*, *18*(7), 955–972. https://doi.org/10.1016/S0883-2927(02)00205-6

Jackson, K. R., & Sacks-Davis, R. (1980). An alternative implementation of variable step-size multistep formulas for stiff ODEs. *ACM Transactions on Mathematical Software*, *6*(3), 295–318. https://doi.org/10.1145/355900.355903

Katona, T., Gilfedder, B. S., Frei, S., Bücker, M., & Flores Orozco, A. (2021). High-resolution induced polarization imaging of biogeochemical carbon-turnover hot spots in a peatland. *Biogeosciences*, *18*(13), 4039–4058. https://doi.org/10.5194/bg-18-4039-2021

Kessouri, P., Furman, A., Huisman, J. A., Martin, T., Mellage, A., Ntarlagiannis, D., et al. (2019). Induced polarization applied to biogeophysics: Recent advances and future prospects. *Near Surface Geophysics*, *17*(6), 595–621. https://doi.org/10.1002/nsg.12072

Kumar, R., Carroll, C., Hartikainen, A., & Martin, O. (2019). ArviZ a unified library for exploratory analysis of Bayesian models in Python. *Journal of Open Source Software*, *4*(33), 1143. https://doi.org/10.21105/joss.01143

Lair, G. J., Gerzabek, M. H., & Haberhauer, G. (2007). Sorption of heavy metals on organic and inorganic soil constituents. *Environmental Chemistry Letters*, *5*(1), 23–27. https://doi.org/10.1007/s10311-006-0059-9

Leroy, P., Revil, A., Kemna, A., Cosenza, P., & Ghorbani, A. (2008). Complex conductivity of water-saturated packs of glass beads. *Journal of Colloid and Interface Science*, *321*(1), 103–117. https://doi.org/10.1016/j.jcis.2007.12.031

Li, L., Sullivan, P. L., Benettin, P., Cirpka, O. A., Bishop, K., Brantley, S. L., et al. (2021). Toward catchment hydro-biogeochemical theories. *WIREs Water*, *8*(1), e1495. https://doi.org/10.1002/wat2.1495

Mellage, A., Dörrich, M., & Haderlein, S. B. (2022a). Capturing in situ glyphosate (De) sorption kinetics in floodplain aquifer sediment columns: Geophysical measurements and reactive transport modeling. *Environmental Science & Technology*, *56*(18), 12955–12964. https://doi.org/10.1021/acs.est.1c07119

Mellage, A., Smeaton, C. M., Furman, A., Atekwana, E. A., Rezanezhad, F., & Van Cappellen, P. (2018). Linking spectral induced polarization (SIP) and subsurface microbial processes: Results from sand column incubation experiments. *Environmental Science & Technology*, *52*(4), 2081–2090. https://doi.org/10.1021/acs.est.7b04420

Mellage, A., Zakai, G., Efrati, B., Pagel, H., & Schwartz, N. (2022b). Paraquat sorption- and organic matter-induced modifications of soil spectral induced polarization (SIP) signals. *Geophysical Journal International*, *229*(2), 1422–1433. https://doi.org/10.1093/gji/ggab531

Patterson, J. W., Allen, H. E., & Scala, J. J. (1977). Carbonate precipitation for heavy metals pollutants. *Journal (Water Pollution Control Federation)*, 2397–2410.

Randhawa, N. S., & Broadbent, F. E. (1965). Soil organic matter-metal complexes: 5. Reactions of zinc with model compounds and humic acid. *Soil Science*, *99*(5), 295–300. https://doi.org/10.1097/00010694-196505000-00002

Revil, A., Cathles, L. M., Losh, S., & Nunn, J. A. (1998). Electrical conductivity in shaly sands with geophysical applications. *Journal of Geophysical Research*, *103*(B10), 23925–23936. https://doi.org/10.1029/98JB02125

Rühlmann, J., Körschens, M., & Graefe, J. (2006). A new approach to calculate the particle density of soils considering properties of the soil organic matter and the mineral matrix. *Geoderma*, *130*(3), 272–283. https://doi.org/10.1016/j.geoderma.2005.01.024

Saneiyan, S. (2019). *Geophysical methods for monitoring soil stabilization by microbial induced carbonate precipitation*. Doctoral thesis. Rutgers University. https://doi.org/10.7282/t3-scpk-bd54

Scheidegger, A. E. (1961). General theory of dispersion in porous media. *Journal of Geophysical Research (1896-1977)*, *66*(10), 3273–3278. https://doi.org/10.1029/JZ066i010p03273

Schwartz, N., & Furman, A. (2014). On the spectral induced polarization signature of soil organic matter. *Geophysical Journal International*, *200*(1), 589–595. https://doi.org/10.1093/gji/ggu410

Schwarz, G. (1962). A theory of the low-frequency dielectric dispersion of colloidal particles in electrolyte solution 1,2. *The Journal of Physical Chemistry*, *66*(12), 2636–2642. https://doi.org/10.1021/j100818a067

Serban, R., & Hindmarsh, A. C. (2008). Cvodes: The sensitivity-enabled ODE solver in SUNDIALS. *Volume 6: 5th International Conference on Multibody Systems, Nonlinear Dynamics, and Control, Parts A, B, and C*, 257–269. https://doi.org/10.1115/DETC2005-85597

Seyboldt, A., Osthege, M., Störiko, A., Widmer, L., Mares, B., & Porter, J. R. (2024). Pymc-devs/sunode: V0.6.0 [Computer Software]. *Zenodo*. https://zenodo.org/records/11187750

Slater, L. D., & Glaser, D. R. (2003). Controls on induced polarization in sandy unconsolidated sediments and application to aquifer characterization. *Geophysics*, *68*(5), 1547–1558. https://doi.org/10.1190/1.1620628

Strobel, C., Abramov, S., Huisman, J. A., Cirpka, O. A., & Mellage, A. (2023a). Spectral induced polarization (SIP) of denitrification-driven microbial activity in column experiments packed with calcareous aquifer sediments. *Journal of Geophysical Research: Biogeosciences*, *128*(1), e2022JG007190. https://doi.org/10.1029/2022JG007190

Strobel, C., Doerrich, M., Stieff, E.-H., Huisman, J. A., Cirpka, O. A., & Mellage, A. (2023b). Organic matter matters—The imaginary conductivity of sediments rich in solid organic carbon. *Geophysical Research Letters*, *50*(23), e2023GL104630. https://doi.org/10.1029/2023GL104630

Strobel, C., Störiko, A., Olaf, O. A., & Mellage, A. (2024). Electronic appendix for are we there yet? A critical experimental assessment of the application of induced polarization for monitoring geochemical processes [Dataset]. *Zenodo*. https://doi.org/10.5281/ZENODO.12788754

Tsukanov, K., & Schwartz, N. (2020). Relationship between wheat root properties and its electrical signature using the spectral induced polarization method. *Vadose Zone Journal*, *19*(1), e20014. https://doi.org/10.1002/vzj2.20014

Vaudelet, P., Revil, A., Schmutz, M., Franceschi, M., & Bégassat, P. (2011). Induced polarization signatures of cations exhibiting differential sorption behaviors in saturated sands. *Water Resources Research*, *47*(2), W02526. https://doi.org/10.1029/2010WR009310

Vehtari, A., Gelman, A., Simpson, D., Carpenter, B., & Bürkner, P.-C. (2021). Rank-normalization, folding, and localization: An improved {{$ \widehat{R}$}} for assessing convergence of MCMC. *Bayesian Analysis*, *16*(2), 667–718. https://doi.org/10.1214/20-BA1221

Weigand, M., & Kemna, A. (2019). Imaging and functional characterization of crop root systems using spectroscopic electrical impedance measurements. *Plant and Soil*, *435*(1–2), 201–224. https://doi.org/10.1007/s11104-018-3867-3

Weller, A., Breede, K., Slater, L., & Nordsiek, S. (2011). Effect of changing water salinity on complex conductivity spectra of sandstones. *Geophysics*, *76*(5), F315–F327. https://doi.org/10.1190/geo2011-0072.1

Zhang, C., Revil, A., Fujita, Y., Munakata-Marr, J., & Redden, G. (2014). Quadrature conductivity: A quantitative indicator of bacterial abundance in porous media. *Geophysics*, *79*(6), D363–D375. https://doi.org/10.1190/geo2014-0107.1

References From the Supporting Information

Bromly, M., Hinz, C., & Aylmore, L. A. G. (2007). Relation of dispersivity to properties of homogeneous saturated repacked soil columns. *European Journal of Soil Science*, *58*(1), 293–301. https://doi.org/10.1111/j.1365-2389.2006.00839.x